Journal of ELECTRICAL ENGINEERING, VOL 74(2023), NO1, 32–39

sciendo

PAPERS

Indicator of the influence of a geomagnetic storm on the transmission electric system

Daniel Mayer[1], **Milan Stork**[2]

Magnetic storms are severe disorders in the Earth's magnetosphere caused by enormous solar activity. The magnetic storm induces a quasi-stationary geomagnetic current (GIC) in the wires of the very high voltage (VHV) lines. These currents cause the current and thus thermal overload of the VHV part of the transmission lines, especially the transformers of the system. In the submitted article described by a device that indicates these effects of magnetic storms on the transmission system and allows it to carry out its safe operation. The indicator is located on the VHV wire of the bundle conductor. Using the Hall probe, it senses the magnetic field of the current in the line. With a digital frequency low-pas filter removes the ac component of the indicated current and information about its dc component, *ie* about the GIC, wireless transmission to the workplace of the system operator. This will then instruct the transmission system protective regime.

K e y w o r d s: magnetic storm, magnetosphere, transmission system, transmission system protection

1 Introduction

Geomagnetic field anomalies, referred to as magnetic storms, can severely disrupt various technical devices. The more advanced technology a person uses, the more vulnerable this technique is, and thus the threat of magnetic storms becomes more relevant. In addition to various technical devices, such as satellite telecommunications networks, navigation systems, but also pipeline networks for the transmission of gases and liquids, *etc* magnetic storms can damage transmission systems, especially power transformers, and cause large power outages. The source of the Earth's magnetic field is both internal, *ie* physical processes inside the Earth, and external, *ie* physical processes in the heliosphere of the Sun, see Fig. 1, [1-3]. The internal source of the Earth's magnetosphere is the currents induced in the moving fluid core of the Earth. The simulation model of this phenomenon is called a magnetohydrodynamic dynamo. This is a complex turbulent flow in which magnetohydrodynamic, and thermal phenomena are applied. It changes with time (this is manifested, for example, by the shifting of the Earth's magnetic poles), but relatively slowly (in the order of years) we talk about secular variations.

The intensity of the internal magnetic field varies with place on Earth. At our latitudes, the magnetic induction has a value of about 44 μT, at the poles around 60 μT and at the magnetic equator around 30 μT. The Earth's external magnetic field has its origins in solar flares, where coronary mass containing electrons and protons erupts. This product is called CMA (Coronal Mass Ejection), so it has its own magnetic field, which then propagates through interplanetary space.

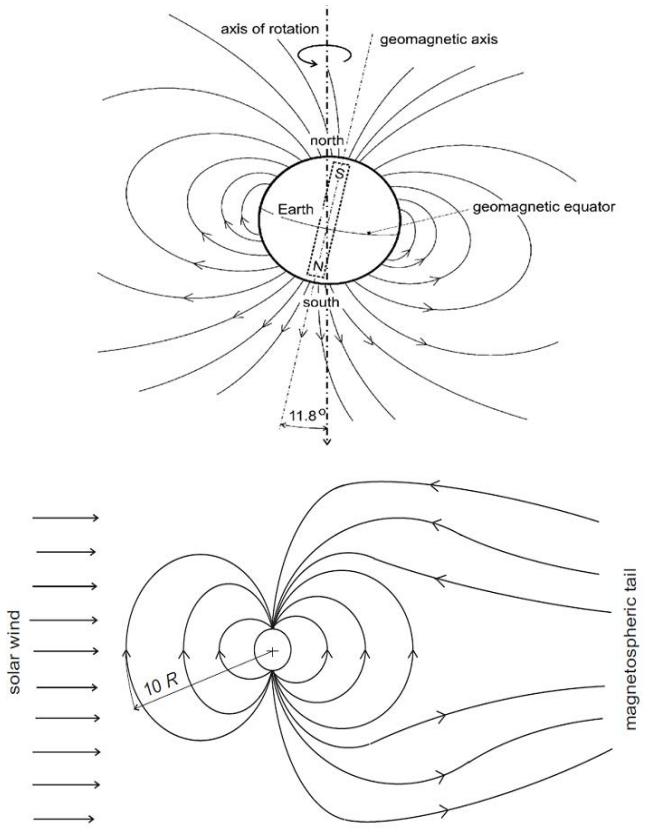

Fig. 1. Earth's magnetosphere: (a) – without the influence of solar activity, (b) – deformed by the effect of solar wind

[1] Department of Electrical and Computational Engineering, University of West Bohemia, Plzen, Czech Republic, mayer@fel.zcu.cz, [2] Department of Electronics and Information Technology, University of West Bohemia, Plzen and research institute RICE in Plzen, Czech Republic, stork@fel.zcu.cz

https://doi.org/10.2478/jee-2023-0004, Print (till 2015) ISSN 1335-3632, On-line ISSN 1339-309X

If the flow of these particles (the so-called solar wind) hits the Earth's magnetosphere, it deforms its shape and partly penetrates into its deeper layers, especially in the magnetic poles, which is reflected in rapid variations in the geomagnetic field (seconds to hours).

Its intensity varies, from minor disturbances (20 to 30 nT) to strong (up to hundreds of nT) magnetic variations caused by a solar wave. They are called magnetic storms, Fig. 1. We cannot influence the possible impact of the Earth's magnetosphere with a significant CMA object with the subsequent formation of a geomagnetic storm. However, we can predict the occurrence of magnetic storms, their size and location on Earth, and if there is a danger of their occurrence, take technical measures to prevent major damage. The geomagnetic field $\boldsymbol{B}(t)$ acting on the conductors of the transmission system induces GIC in them as

$$rot\boldsymbol{E}(t) = -\frac{\partial \boldsymbol{B}(t)}{\partial t}, \quad \boldsymbol{J}(t) = \gamma \boldsymbol{E}(t), \tag{1}$$

where $\boldsymbol{E}(t)$ is the intensity of the electric field, γ is the conductivity and $\boldsymbol{J}(t)$ is the density of GIC. According to the law of electromagnetic induction, their magnitude depends on the derivative of the magnetic induction, so only the external magnetic field applies.

The quantity $\boldsymbol{B}(t)$ and therefore also the GIC have a random time course. Although rapid variations are mentioned, they change relatively slowly (in nT/min), compared to industrial frequency alternates; we call them quasi-stationary. Depending on the time, GICs behave like direct currents. Thus, only the ohmic resistances of the system conductors affect the GIC distribution in the transmission system, while the inductances and capacitances of the electrical network do not apply.

In works [4-16] it was proved that the immediate cause of transmission system failures are these GIC induced in the HV transmission line. These currents cause the phenomenon of semisaturation, *ie* half-period supersaturation of the magnetic circuit of the power transformers, which results in current and consequently thermal overload of their VHV windings. Monitoring the size of the GIC in the VHV line is therefore essential for the protection of power transformers.

2 Monitoring of geomagnetic field and later GIC in VHV line

The Earth's magnetic field is monitored by a worldwide network of geomagnetic observatories. All three components of the geomagnetic induction vector space are measured continuously. The measured values are registered, at an interval of 1 min, or at second intervals, with an accuracy of 0.1 nT. The results are then passed on to the World Data Center in Boulder (USA) and the Edinburgh Geomagnetic Information Node (Scotland). The Space Weather Prediction Center (SWPC) publishes a three-day space weather forecast. The results are freely available on the Internet.

In addition to continuous monitoring of the geomagnetic field, solar activity is constantly monitored. In addition to observing solar flares with solar telescopes, these phenomena are constantly monitored by satellites. One of the first satellites to study the Sun and space weather is the Solar and Heliospheric Observatory (SOHO) probe. At the time of detection of the coronary mass (CMA) heading for the Earth, a calculation is made at the Goddard Space Flight Center (GSCF) to determine the density at which it will hit the Earth's magnetosphere and predict the intensity and location of the magnetic storm on Earth. This information is passed on to the power system operators. This work describes a device that can be used to obtain data on the immediate impact of the transmission system by a magnetic storm.

3 Indicator of direct effect of magnetic storm on the transmission system

While current methods of magnetic storm monitoring are only an approximate prediction, the indicator described below provides accurate data at a much lower cost. The transmission of electricity takes place via external HV lines, bundled conductors. The conductors of the bundle form the core of the rope, around which there are electrical conductors in several layers, forming the sheath of the rope, Fig. 2. The core consists of galvanized steel wires, ensuring the mechanical safety of the rope. The casing is usually made of aluminum alloy or copper. In addition to wires of circular cross-section, wires of trapezoidal cross-section, so-called segment conductors, are used, Fig. 3.

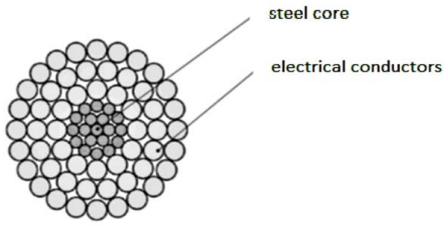

Fig. 2. Aluminium-conductor steel-reinforced (AlFe)

Fig. 3. Cable composed of segmented conductors, (trapeziodal wire)

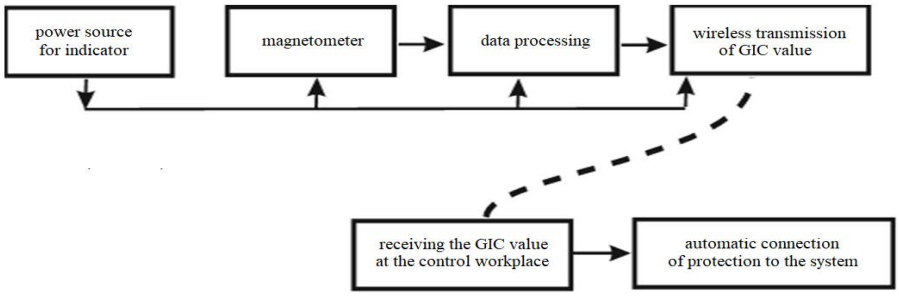

Fig. 4. Main parts of indicator

The indicator is located in close proximity to one of the HV beam conductors through which the current passes

$$i(t) = i_{\mathrm{p}}(t) + I_{\mathrm{s}}. \tag{2}$$

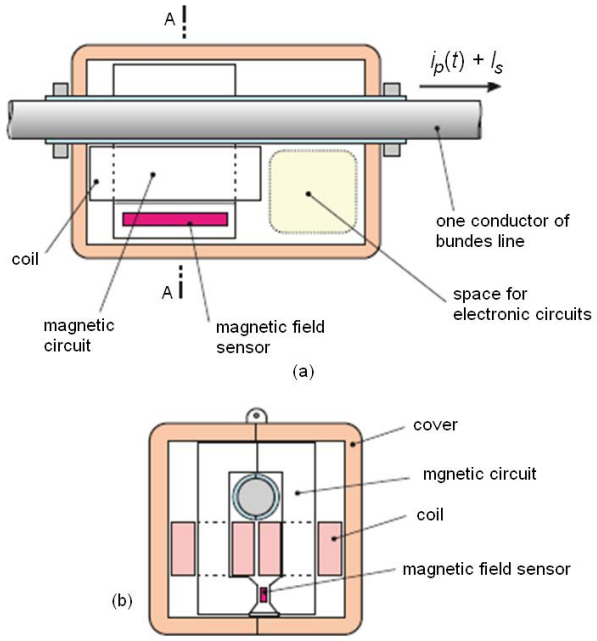

Fig. 5. Overall arrangement of the indicator: (a) – longitudinal cut, (b) – cut A-A

The current $i_{\mathrm{p}}(t)$ is supplied by the power plant and the quasi-stationary current I_{s} is generated by a magnetic storm. The indicator measures the current $i(t)$. The indicator has the following parts, Fig. 4:

- Energy source of the indicator is energy converter from the HV conductor for powering other parts of the indicator. The magnetic field $B(t)$ of the current $i(t)$ is closed (passed) by a magnetic circuit with a coil, into which a voltage is induced, which is then adjusted (rectified, stabilized and filtered).
- A magnetometer with a Hall probe, *ie* a magnetic field sensor $B(t)$, which is proportional to the current $i(t)$ passing through the conductor.
- A circuit for processing data from a magnetometer. A low-pass filter suppresses the AC component of the current $i(t)$ and passes only the DC component I_{s} The output voltage of the Low-pass filter corresponds to the current I_{s}.
- Transmission system. Sampled current values I_{s} and $i(t)$ are wirelessly transmitted to the operator's workplace.
- Reception and interpretation of I_{s} values in the control workplace. If it reaches a certain, preset value, it automatically activates protective measures that face damage to the power transformer of the transmission system (see *eg* [7])

The overall design of the indicator is shown in Fig. 5.

3.1 Magnetometer data processing circuit

The low-pass filter suppresses the first harmonic in the current $i(t)$ and passes the current I_s. Information about the current value is then wirelessly transmitted to the control workplace. When they reach certain, preset values, it automatically activates protective measures that prevent damage to the power transformer of the transmission system. The indicator is structurally designed so that it is only "hung" on one of the conductors of the VHV harness during installation and its position is then automatically locked. Its implementation in the transmission system can be done by a line that is in full operation, *ie* live, using a drone. The indicator can be removed from the wire in a similar way. The indicator does not require maintenance or service, it works automatically. The indicator is designed to face safely:

- Outdoor weather conditions, especially rain, fog, icing, wind, *etc*.

- Ambient temperature ranging from -50 to +125 °C.

- Its shape prevented the formation of the corona, or other forms of non-independent electric discharge, which phenomena occur in places of non-smooth surface and in parts with sharp edges.

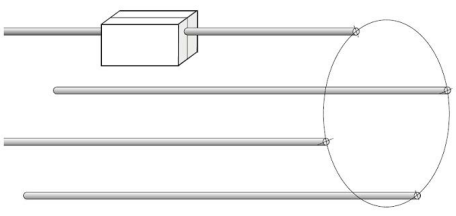

Fig. 6. Location of the indicator on the wire of bundle line

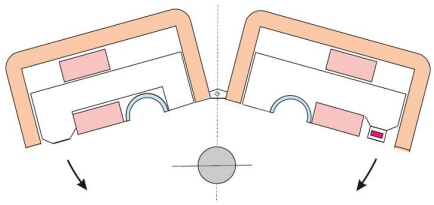

Fig. 7. Inserting an indicator on the wire of a bundle line

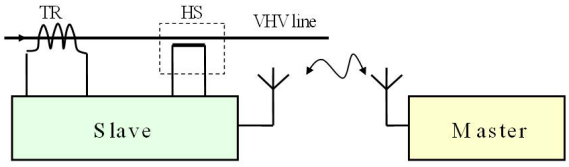

Fig. 8. Wireless communication between the master and slave blocks of GIC

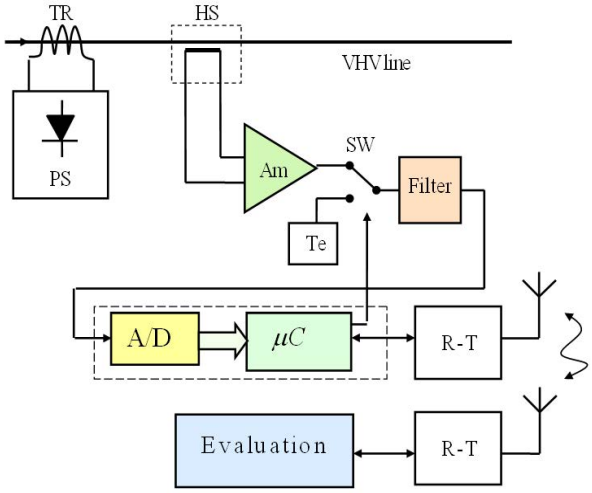

Fig. 9. The block diagram of the indicator with analog low-pass filter: TR–transformer, PS–power supply, VHV–high voltage line, HS–Hall effect sensor, Am–amplifier, Te–testing circuit, SW–electronic switch, Filter–analog lowpass filter, A/D–analog/digital converter, μC–microcontroller, R-T–receiver/transmitter, Evaluation block

Installation/disassembly of the indicator on the conductor of the line (Fig. 6) can be done either manually or by a drone. When inserted on the conductor, the open indicator (Fig. 7), suspended on the drone handling arm, approaches the wire in the vertical direction. Then the two parts of the indicator are connected and detached from the shoulder of the drone. When shooting an indicator from the wire, the drone is connected between the drone arm and the indicator by means of a steel plate on the upper part of the indicator and a plate permanent magnet. The grip of both parts of the indicator unlocked, the indicator opens, and the vertical pull is removed. The device that ensures this mechanism is carried out using standard design methods and therefore is not described here.

4 Electronic parts of the indicator

The electronic part of the system consists of two parts. The first block master - evaluates the dc component of the current in the line and is located near the operator. The second slave block - is located on the VHV line from which it obtains energy for its operation using a TR transformer and information on the AC and DC current in the Hall probe line. Two-way wireless communication takes place between the Master and Slave blocks, see Fig. 8.

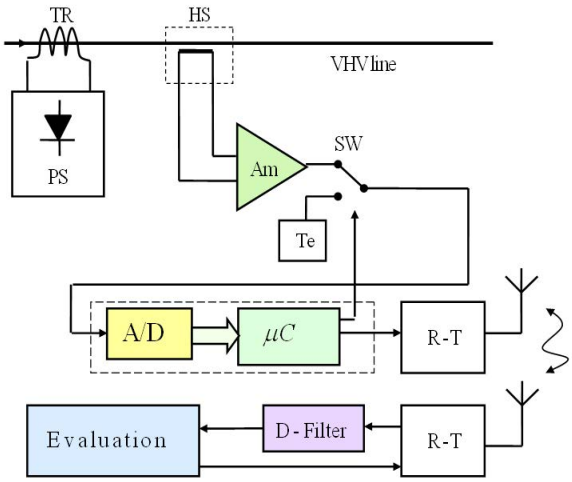

Fig. 10. The block diagram of the indicator with digital low-pass filter: TR–transformer, PS–power supply, VHV–high voltage line, HS–Hall effect sensor, Am–amplifier, Te–testing circuit, SW–electronic switch, A/D–analog/digital converter, μC–microcontroller, R-T–receiver/transmitter, D–Filter-digital lowpass filter

Two versions of dc signal detection in the line are described. Fig. 9 is a block diagram of a first version of a system with an analog low pass filter for evaluating the dc component of a signal on the transmitter side. Fig. 10 is a block diagram of a second version of a system with a digital low-pass filter for evaluating the dc signal component connected on the evaluation side.The part of the device that is located on the VHV conductor (Slave part) is supplied with alternating current which passes through the VHV conductor. The power supply (PS block) contains a transformer, rectifier, switched-mode power supplies which generate the required stabilized voltages with high efficiency. The signal proportional to the AC and DC current in the conductor is obtained by the Hall sensor (HS). The signal from the HS is amplified using the instrument operational amplifier (Am). The output of the amplifier is fed to the switch (SW), to which the test signal from the test circuit (Te) is also fed. The switch is controlled by a microcontroller (C) and test if the device functions properly. In the device according to Fig. 9, the output of the SW is connected to an analog low-pass filter and its output to an analog-to-digital A/D converter, which is a part of C. The device is supplemented by a transceiver (R-T block), which communicates wirelessly

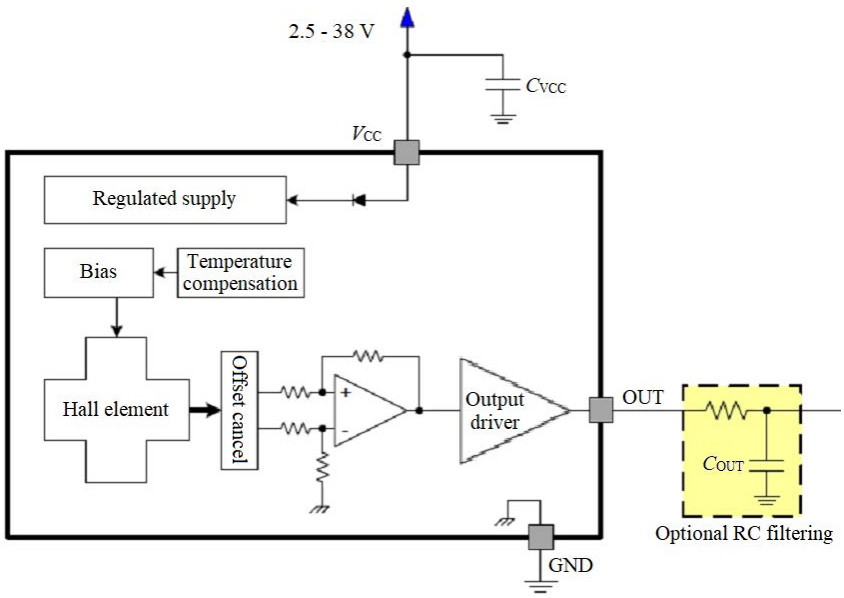

Fig. 11. Wire diagram of Hall effect sensor [17]

with the second part of the device, which also contains a transceiver and an evaluation block, which in the case of the dc component in the line notifies the operator. The only difference in the device according to Fig. 10 is that it does not contain an analog filter, but the signal from the amplifier Am is fed to the A/D converter via the SW switch. In this case, a signal containing the ac and dc components is transmitted. The second part of the device then evaluates the data using a digital low-pass filter (D - filter). The advantage of the first solution is the direct evaluation of the dc component using an analog low-pass filter and the transmission of only this signal to the master. The advantage of the second system is that information about the AC and DC current component in the conductor is transmitted to the master, and the evaluation is then performed from the received samples in a digital way. It should be noted that in order to increase the error tolerance, it is advisable to transmit the sampled data from the Hall probe, as well as the sampled data from the output of the analog low-pass filter.

5 Design of the indicator

In this section, some electric and electronic components for the indicator are specified in more detail, as well as the preliminary weight of the indicator. Suppose one conductor of the bundle line: diameter 12 mm. The current flowing through this conductor consists from AC current (*eg* 100 A) and GIC current (*eg* 5 A)

$$i(t) = \underbrace{I_{\mathrm{m}} \sin(\omega t)}_{\mathrm{AC}} + \underbrace{I_{\mathrm{s}}}_{\mathrm{GIC}} = 100\sqrt{2}\sin(\omega t) + 5. \qquad (3)$$

The maximum instantaneous current $i(t)$ is therefore approximately 150 A. However, it is necessary to calculate the output voltage for the AC current and the GIC current in order not to over-saturate the probe. The following type of Hall probe DRV5053 is assumed to be used - Analog-Bipolar Hall Effect Sensor [17], wire diagram is shown in Fig. 11.

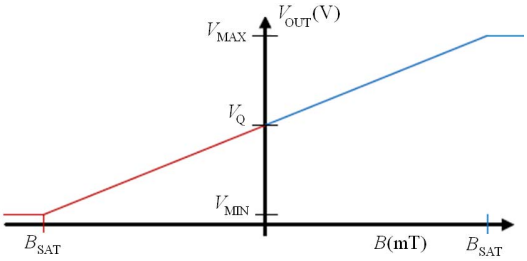

Fig. 12. Voltage output of Hall effect sensor DRV5053 Positive Sensitivity [17]

The DRV5053 device is a chopper-stabilized Hall IC that offers a magnetic sensing solution with superior sensitivity stability over temperature and integrated protection features. A wide operating voltage range from 2.5 to 38 V. The 0 to 2 V analog output responds linearly to the applied magnetic flux density, and distinguishes the polarity of magnetic field direction (for $B = 0$, output voltage = 1 V). The minimum unsaturated output voltage (min) $B < B_{\mathrm{S}}$ is 0.2V and the maximum unsaturated output voltage (max) is $B > B_{\mathrm{S}}$ is 1.8V, see Fig. 12.

Hall effect sensors are produced with the following sensitivities [17]: 11 mV/mT, 23 mV/mT, 45 mV/mT, 90 mV/mT, +23 mV/mT, +45 mV/mT.

We expect the maximum value of the current, $I_{\max} = 150\mathrm{A}$. Magnetic fields in the area of the Hall probe, induced for the current - approximate calculation:

$$\oint_C \boldsymbol{H} \cdot d\boldsymbol{l} = I. \qquad (4)$$

Only air gaps $l_1 = 1\,\mathrm{mm}$ and $l_2 = 8\,\mathrm{mm}$ are applied when neglecting the magnetic resistance of iron. Magnetic

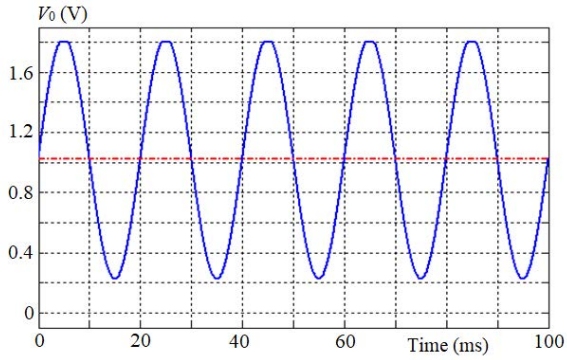

Fig. 13. Blue line - limited signal from Hall effect sensor, red line - mean voltage

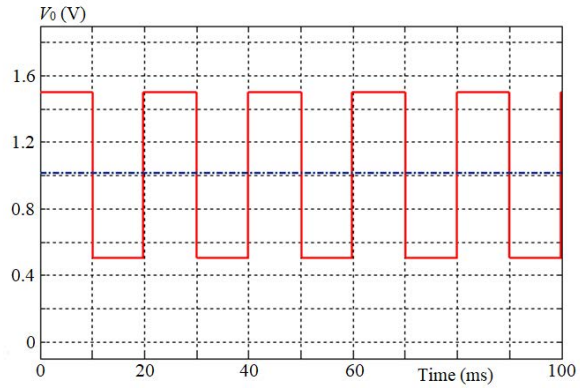

Fig. 14. Red curve - limited signal, black line - mean voltage 1.012 (0.012 V due to GIC)

intensity is $H = I/(l_1 + l_2) = 1.66 \times 10^4$ and magnetic induction is $B = \mu_0 H = 0.021\,\mathrm{T}$. Since the Hall effect sensor can have a sensitivity of up to 45 mV/mT, the output voltage (with offset voltage $V_{\mathrm{off}} = 1\mathrm{V}$) will be $V\mathrm{out} = 1.945\,\mathrm{V}$. This means that the probe is in saturation (because output voltage $> 1.8\,\mathrm{V}$) therefore probe with a lower sensitivity must be taken, *ie* +23 mV/mT, providing 1.483 V output.

The result shows that the sensitivity of this probe is satisfactory. In a similar way, the output voltage of the Hall probe can be checked only for the current due to the GIC. Now it is also possible to calculate the output voltage of the indicator only for the GIC current, since the AC component is suppressed by a low-pass filter (analog or digital). We expect the minimum value of the GIC current, $I_{\mathrm{s}} = 5\mathrm{A}$, to which the indicator should already respond. Magnetic fields in the area of the Hall effect probe, induced only by the GIC current is $I_{\mathrm{s}} = 5\mathrm{A}.1$ For this GIC current, according to (5) and (6), the magnetic intensity $H \approx 5.6 \times 10^2$ A/m and magnetic inductance $B \approx 0.7$ mT. For a Hall effect sensor with a sensitivity of 23 mV/mT, the output voltage of the sensor will be about 1 V.

In the previous section, a Hall effect probe was selected with such gain that, if possible, the output signal of the probe was not limited. Nevertheless, under certain circumstances, a limitation may occur. It can be proven that even in the case of signal limitation, if a suitable method of evaluation is used, the indicator will work correctly.

Assume a current according to the relation (3). This current is processed by a Hall probe, where the output signal is limited, see Fig. 13

The signal can be trimmed by symmetrically limiting around 1 V, and then by passing the signal through a low-pass filter, the mean value of the signal is obtained, which gives the GIC value, see Fig. 14.

The result shows that even in the case of a limited signal, information about the GIC component of the current can be obtained. An important part in signal evaluation is the low-pass filter. A switched-capacitor filter can be used for the analog version. The MAX291 is Butterworth 8th-order, low-pass, switched-capacitor filter that can be set up with corner frequencies from 0.1Hz to 25kHz [18]. The corner frequency of the low-pass filter is controlled by changing the clock frequency, which is 100 times higher than the required corner frequency. The connection of the low-pass filter is shown in Fig. 15. The STM32F303K8 C with 12 bit A/D converter was used in indicator [19 - 21].

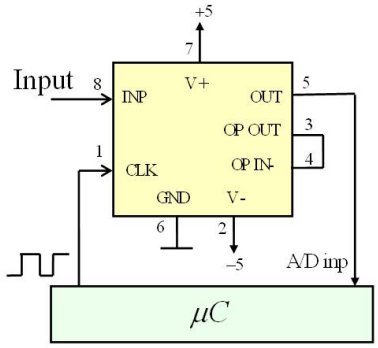

Fig. 15. Example of low-pass filter connection where corner frequency is controlled by μC

The approximate weight of the indicator, where the main items are the following parts: Magnetic circuit 0.86 kg, coils 0.81 kg, housing 0.27 kg, weight of electronics 0.20 kg. The total weight of the indicator is 2.14 kg The indicator is equipped with a device that firmly locks the body of the indicator to the wire after inserting the indicator onto the wire. This device also enables easy disassembly, *ie*the vertical pull of the indicator body cancels the arrest, which enables easy removal of the indicator. This design is made by standard construction methods and is therefore not presented here.

6 Wireless data transfer

The sampling frequency of analog signals was chosen to be 500 Hz (*ie* 10 times higher than the mains frequency). A digitized Hall probe signal (2 bytes), a digitized low-pass filter signal (2 bytes) and 2 bytes for optional indicator status information are transmitted. If is

assumed transmission in the form of comma-separated values (CSV) + carriage return (CR) + line feed (LF), it is a total of 11 bytes. After completing each byte with a start and stop bit, the transfer rate must be: Data_Rate= $10 \dots 11 f_s$ giving 55000 bit/s, at the given sampling frequency. It is possible to choose the next higher standard baud rate, which is 57600 bit/s or 115200 bit/s. Several modules have been tested for wireless data transmission, *eg* HC - 05 Bluetooth Module [22], RFM01, RFM02 Modules [23, 24] and nRF24L01+, Single Chip 2.4GHz Transceiver [25]. The best results were achieved with the nRF24L01, which has the following features:

Range depending on the transfer speed - for 2MB rate (Open area): 520m, for 1MB rate (open area): 750 m, for 250pKb rate (open area): 1000 m weight: 25.0 g, board size: 4.6 ...1.7...1.2 cm.

7 Conclusion

The described device allows online monitoring how the geomagnetic field disorders (magnetic storm) act on the transmission electrical system. If there is a risk of damage to the highvoltage part of the system, the protective devices *eg* [7], can be automatically or manually connected to the system and thereby convert to the safety mode of the system. The indicated indicator has the following advantages:

- is both production and cost-effective;
- is robust (reliable), practically trouble-free and has a very long life;
- does not require operation or maintenance, can be involved in automatic control;
- its implementation into the system, *ie* its assembly and disassembly at any point in the VHV line is easy and can be done in full operation of the system;
- is also safe health with regard to high voltage guidance, ecologically is completely neutral;
- indicates virtually immediate response between GIC's action in the system and displaying GIC at the management workplace.

Acknowledgements

This work was supported by Department of Electrical and Computational Engineering and Department of Electronics and Information Technology/RICE, University of West Bohemia, Plzen, Czech Republic and by the Ministry of Education, Youth and Sports of the Czech Republic under the project OP VVV Electrical Engineering Technologies with High-Level of Embedded Intelligence, CZ.02.1.01/0.0/0.0/18_069/0009855 and by the Internal Grant Agency of University of West Bohemia in Plzen, the project SGS-2021-005.

References

[1] E. N. Parker, *Cosmical magnetic fields*, Oxford, Clarendon Press, 1979.

[2] E. Priest, *Solar magnetohydrodynamics*, Dordecht, D. Reidel Publia Co., 1984.

[3] R. R. Benestand, *Solar activity and Earths climate*, Berlin, Springer-Verlag,2003.

[4] R. Girgis, "Effects of geomagnetically induced currents on power transformers and power systems", *CIGRE*, 21, rue dArtois, F-75008 Paris, A2-304, pp. 1-8.

[5] D. Mayer, "Contribution to investigation of influence of geomagnetic stroms on electrification system", *Acta Technica*, vol. 58, no. pp. 351-365, 2013.

[6] M. Stork and D. Mayer,"Direct currents in power transformers", *Journal of El. Eng*, vol. 70, no. 1, pp. 68-72, 2019.

[7] D. Mayer,"Protection of power transformers against the effect of magnetic storms", *Journal of El. Eng.*, vol. 72, no. 4, pp. 249-255, 2021.

[8] L. J. Lanzerotti,"Space weather effects on technologies", *Song P. et al(eds.): Space Wheater, American Geophysical Union, Geophys*, Monograph. 125, pp. 11-25, 2001.

[9] R. Nishiura, S. Yamashita and S. Kano,"Simulation analysis of geomagnetically induced currents (GIC) effects on shell-form transformers", *Power and Energy Society General Meeting*, PES IEEE, pp. 21-25, July 2013.

[10] K. J. Patel,"An analytic review of geomagnetically induced current effects in power system", *Internet. Conf. on Electrical, Electronics and Optimization Techniques*, ICEEOT, IssueData, 3-5 March 2016.

[11] J. R. Niño,"Core saturation effect of geomagnetic induced currents in power transformers", *Journal of Applied Research and Technology*, vol. 14, pp. 87-92, 2016.

[12] D. Mayer,"The effect of geomagnetic storms on the electrification system", *Cyclonic and Geomagnetic Storms, Predicting factors, formation and enviromental impacts*, Editor: Victoria P. Banks, Nova Science Publishers, Inc. New York, pp. 1-18, isbn: 978-1-63482-360-9, 2015.

[13] F. Bachinger *et al*," Direct current in transformers: effects and compensation" *CIGRE*,.

[14] J. Ramírez-Niño *et al*,"Core saturation effect of geomagnetic induced currents in power transforms", *Journal of Applied Research and Technology*, vol. 14, pp. 87-92, 2016.

[15] R. Price,"Geomagnetically induced currents effects on transformers", *IEEE Transactions on Power Delivery*, vol. 17, no. 4, pp. 1002-1008, October 2003.

[16] L. Bolduc *et al*,"Development of a DC current-blocking device for transformer neutrals", *IEEE Trans. on Power Delivery*, vol. 20, no. 1, pp. 163-168, Jan 1995.

[17] DRV5053,"Analog-Bipolar Hall Effect Sensor", *Texas Instruments*, SLIS153C May 2014Revised Dec 2015.

[18] MAX 291,"8th-Order, Lowpass, Switched-Capacitor Filters", *Maxim New Releases Data Book*, vol. II, pp. 6-31- 6-46, 1993.

[19] "STM32F303x6/x8, stm32f303c6-1, DS9866 Rev 8", *Available on*, www.st.com, 2018.

[20] "AN4776", *General-purpose timer cookbook*, DocID028459 Rev 2, May 2017.

[21] "STM32 Nucleo-32 boards, UM1956", *User manual.*

[22] "HC - 05 Bluetooth Module, Users Manual V1.0", ,.

[23] "HOPE MICROELECTRONICS CO., LTD. RFM02,Universal ISM Band FSK Transmitter", [*online*], https://www.tme.eu/Document/648e17cf6585c8a49f7dbc75bc074706/RFM02-433-D.pdf, 2006.

[24] "HOPE MICROELECTRONICS CO., LTD. RFM01, Universal ISM Band FSK Receiver", [*online*], https://www.tme.eu/Document/12638ea34a59443d6d7a7e6951bede32/RFM01-433-D.pdf, 2006.

[25] "nRF24L01+, Single Chip 2.4GHz Transceiver, Preliminary Product Specification v1.0, Nordic Semiconductor" [*online*], https://www.sparkfun.com/datasheets/Components/SMD/nRF24L01Pluss Preliminary_Product_Specification_v1_0.pdf.

Received 31 October 2022

Daniel Mayer, Prof, Ing, DrSc received the Ing, PhD and DrSc degrees in electrical engineering from Technical University in Prague, Czech Republic. In 1959 Associate Professor at the University of West Bohemia in Pilsen, in 1968 full Professor of the Theory of Electrical Engineering. Many years he was head of the Department of Theory of Electrical Engineering. Research interests: circuit theory, electromagnetic field theory, electrical machines and apparatus, history of electrical engineering. He published 9 books, more than 350 scientic papers and 15 patents. He is a member of editorial boards of several international journals and leader of many grant projects.

Milan Stork received the MSc degree in electrical engineering from the Technical University of Plzen, Czech Republic at the department of electronics in 1974 and PhD degree in automatic control systems at the Czech Technical University in Prague in 1985. In 1997, he became as Associate Professor at the Department of Electronics and Information Technology, faculty of electrical engineering on University of West Bohemia in Pilzen, Czech Republic and full professor in 2007. He has numerous journal and conference publications. He is member of editorial board magazine"Physician and Technology". His research interests include analog/digital systems, signal processing and biomedical engineering, especially cardiopulmonary exercise tests systems.